Electronic Supplementary Material (ESI) for Nanoscale.
This journal is © The Royal Society of Chemistry 2022

Supporting Information

Plasma synthesis of defects-rich flexible carbon cloth decorated with PtRu alloyed nanoclusters for highly efficient pH-universal electrocatalytic hydrogen evolution

Jingsen Zhang[a], Xiuling Zhang[b], Chuan Shi[a], Guangqing Xia[c,d], Hong Li[b], Peng Wang[b], and Lanbo Di[b,c,d,*]

[a] State Key Laboratory of Fine Chemicals, College of Chemical Engineering, Dalian University of Technology, Dalian 116024, China

[b] College of Physical Science and Technology, Dalian University, Dalian 116622, China

[c] State Key Laboratory of Structural Analysis for Industrial Equipment, Dalian University of Technology, Dalian 116024, China

[d] Key Laboratory of Advanced Technology for Aerospace Vehicles of Liaoning Province, Dalian University of Technology, Dalian 116024, China

Chemicals: Chloroplatinic acid hexahydrate ($H_2PtCl_6 \cdot 6H_2O$, AR, Pt≥37.5%) was purchased from Tianjin Kermel Chemical Reagent Co. Ltd.. Ruthenium trichloride ($RuCl_3$) was purchased from Henan Psai Chemical Products Co. Ltd.. Nafion solution (5 wt%) was bought from Sigma-Aldrich Chemical Reagent Co. Ltd.. Pt/C catalyst (20 wt%) and carbon cloth (CC) were supplied by Shanghai Hesen Electric Co. Ltd.. All the chemicals were used as received without further purification.

Characterization: X-ray diffraction (XRD) analysis was recorded on a DX-2700 X-ray diffractometer (Dandong Haoyuan Instrument Co. Ltd., China) operated at 40 kV and 30 mA with Cu Kα radiation (λ = 0.154178 nm) in the 2θ ranges from 5° to 90°. The superficial chemical states were collected by an ESCALAN250 X-ray photoelectron spectrometer (Thermo VG, Waltham, MA, USA) with an X-ray source (photon energy 1486.6 eV, 150 W) equipped with a monochromatic Al target. All of the spectra were calibrated by C1s spectrum at 284.6 eV. Scanning electron microcopy (SEM) images was obtained using a TESCAN MIRA4 scanning electron microscopy with an accelerating voltage of 200 eV-30 keV equipped with an EDS detector. The Pt and Ru contents of samples were determined by a Thermo ICAP PRO inductively coupled plasma optical emission spectrometer (ICP-OES). Transmission electron microcopy (TEM), high-resolution TEM (HRTEM) images, selected area electron diffraction (SAED) patterns, scanning transmission electron microscopy (STEM) images, line-scan patterns and the corresponding energy-dispersive X-ray spectroscopy (EDS) mapping images were recorded on a FEI talos F200x G2 transmission electron microscope. The chemical bonding states and compositions of the samples were investigated on a Thermo Scientific Nicolet iS20 Fourier transform infrared spectroscopy (FT-IR) in the range of 4000-

400 cm^{-1}. Raman spectra were collected on a HORIBA Scientific LabRAM HR Evolution microscopic confocal laser Raman spectrometer with 532 nm as the excitation laser.

Electrochemical Measurements: The electrochemical measurements were carried out by using a CHI 760E electrochemical workstation (CH Instruments, Inc., Shanghai) in a standard three-electrode system. The synthesized sample (1× 1.5 cm^2) as working electrode was coupled with Hg/HgO (1M KOH) and graphite rod served as reference and counter electrodes, respectively. The self-supported electrode was used as the working electrodes. Prior to the test, all of the electrolytes were bubbled with high-purity N_2 for at least 30 min to remove the dissolved oxygen, and the electrochemical data were obtained until the stable current density was kept through CV measurements in alkaline and neutral media. Polarization curves were obtained using linear sweep voltammetry (LSV) with a scan rate of 5 $mV \cdot s^{-1}$. Stability tests were measured by CV and chronopotentiometric methods. Electrochemical impedance spectroscopy (EIS) was measured at a frequency ranging from 0.1 Hz to 100 kHz to investigate the charge transfer rate of a material in alkaline and neutral electrolyte medium. CV measurements operated at various scan rates from 20 to 100 $mV \cdot s^{-1}$ were performed to estimate the double-layer capacitance (C_{dl}) of the catalysts. All potentials measured were calibrated to RHE using the following equation.

Alkaline (1.0 M KOH):

$$E_{RHE} = E_{HgO} + 0.0592 \times pH + 0.098\ V$$

Neutral (1.0 M PBS) and acid (0.5 M H_2SO_4):

$$E_{RHE} = E_{SCE} + 0.0592 \times pH + 0.244\ V$$

The Turnover Frequency (TOF) value was calculated by the following equation:[1-3]

$$TOF(s^{-1}) = \frac{j \times A}{2nF}$$

where j is the measured current density at a given overpotential based on the polarization curve, A is the geometric surface area of working electrode (1 cm^2 in this work), F is the Faraday constant (96485 $C \cdot mol^{-1}$), and n is the moles of noble metal on the working electrode (based on the Pt, Ru contents obtained by ICP-MS results).

The mass activity was calculated by the following equation:[4, 5]

$$Mass\ activity(A/mg) = \frac{j \times A}{m}$$

where j is the measured current density at a given overpotential based on the polarization curve, A is the geometric surface area of working electrode (1 cm^2 in this work), m is the moles of noble metal on the working electrode (based on the Pt, Ru content obtained by ICP-MS). DFT calculation methods:

Vienna Ab initio Simulation Package (VASP) with the projector augmented wave (PAW) method were employed to implement the DFT calculations.[6, 7] The exchange-functional was treated using the generalized gradient approximation (GGA) of Perdew-Burke-Ernzerhof (PBE) functional. The Spin-polarizations were carried out for all calculations. The energy cutoff for the plane wave basis expansion was set to 450 eV and the force on each atom less than 0.05 eV/Å was set for convergence criterion of geometry relaxation. The Brillouin-zone integration was sampled by 2×2×1 point. A convergence energy threshold of 10^{-5} eV was applied for the self-consistent calculations. The DFT-D3 method was employed to consider the van der Waals interaction. A 18Å vacuum was added along the z direction in order to avoid the interaction between periodic structures.

The free energies of each key HER intermediates the were calculated by the equation: [8-10]

$$\Delta G = \Delta E_{DFT} + \Delta E_{ZPE} - T\Delta S$$

where ΔE_{DFT} is the DFT electronic energy difference of each step, ΔE_{ZPE} and ΔS are the correction of zero-point energy and the variation of entropy, respectively, which are obtained by vibration analysis, T is the temperature (T = 300 K). Additionally, U correction was adopted for Pt atom (4.26 eV) and Ru atom (3.95 eV).

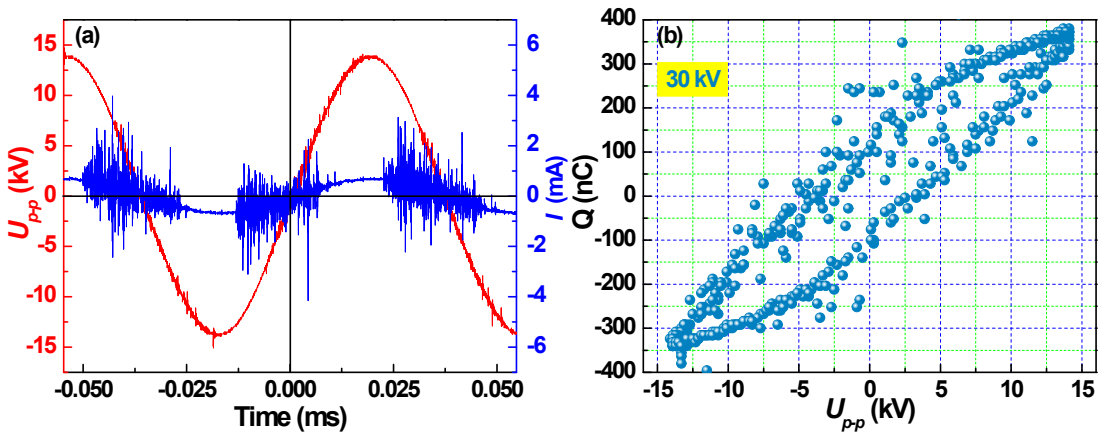

Fig. S1. (a) Discharge voltage and current waveforms, and (b) the corresponding Lissajous Figures of 30%O_2/Ar cold plasma at a discharge voltage of 30 kV and a discharge frequency of 13.6 kHz for treating CC.

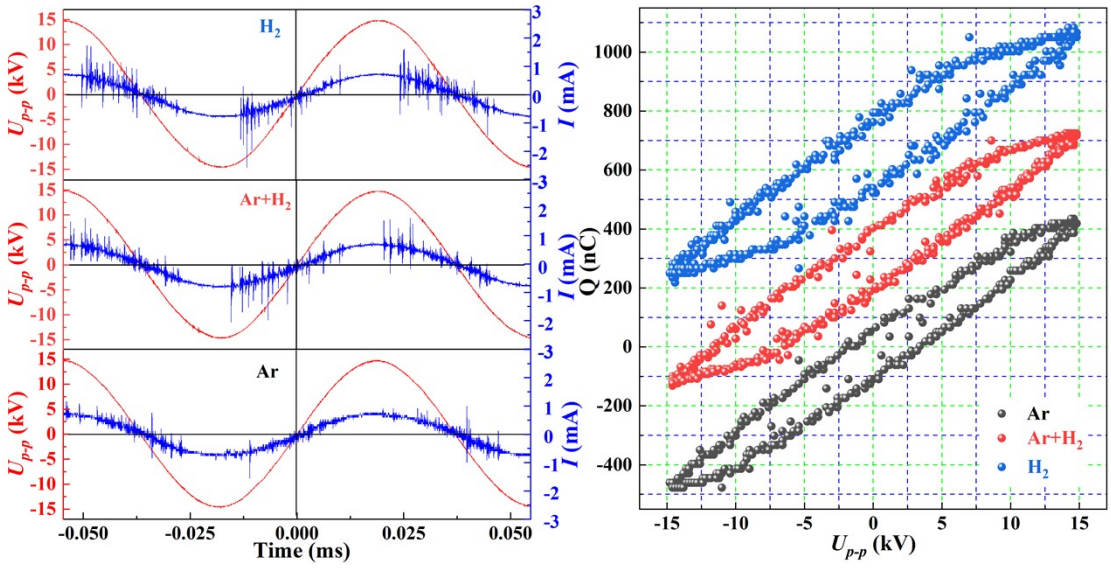

Fig. S2. (a) Discharge voltage and current waveforms, and (b) the corresponding Lissajous Figures of 50%H_2/Ar cold plasma at different discharge voltages (24, 30 and 36 kV) with a discharge frequency of 13.6 kHz for treating PtRu/CC-P.

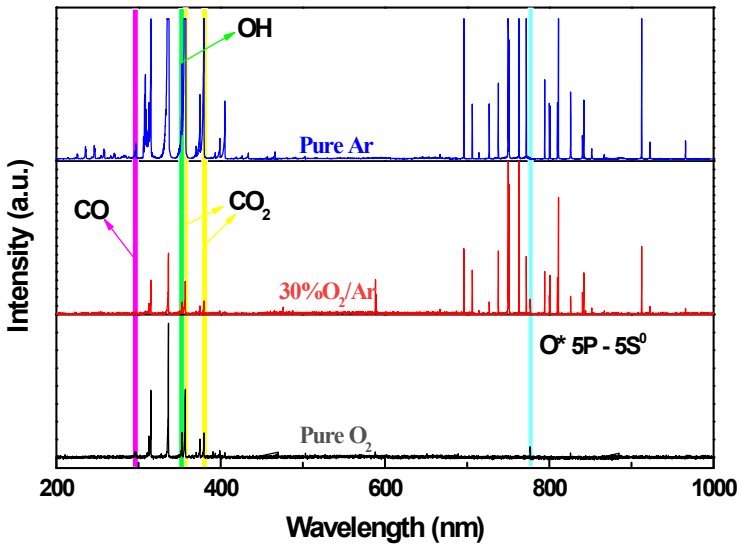

Fig. S3. The optical emission spectra of DBD cold plasma under discharge gases of pure Ar, 30%O_2/Ar and pure O_2.

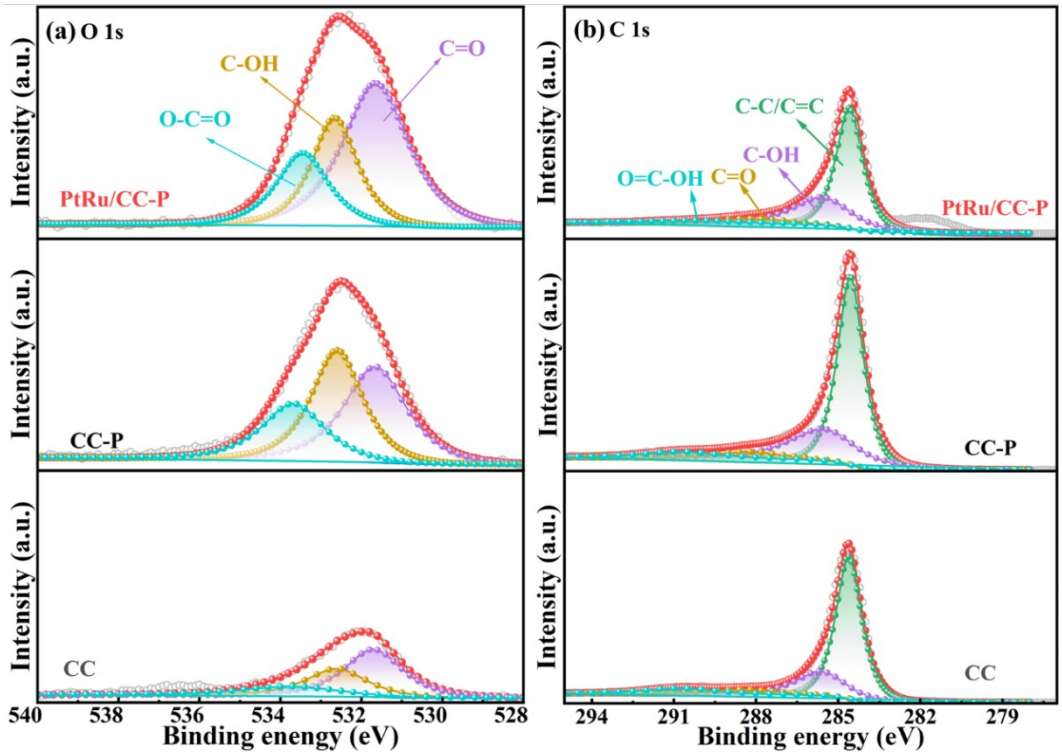

Fig. S4. (a) O1s, and (b) C1s XPS spectra of PtRu/CC-P, CC-P and CC.

In the O1s XPS spectra (Fig. S4a), three peaks can be resolved at 531.2, 532.6 and 533.3 eV, attributing to C=O, C-OH and O-C=O, respectively.[9, 11, 12] Similarly, three peaks at 285.6, 288.3, and 290.8 eV can be divided for the C1s XPS spectra (Fig. S4b), corresponding to C−OH, C=O, and O=C−OH, respectively, whereas a peak at 284.6 eV was ascribed to C-C/C=C.[13, 14] One can see the amount of oxygen-containing functional groups increased obviously for the CC-P after O_2 plasma treatment.

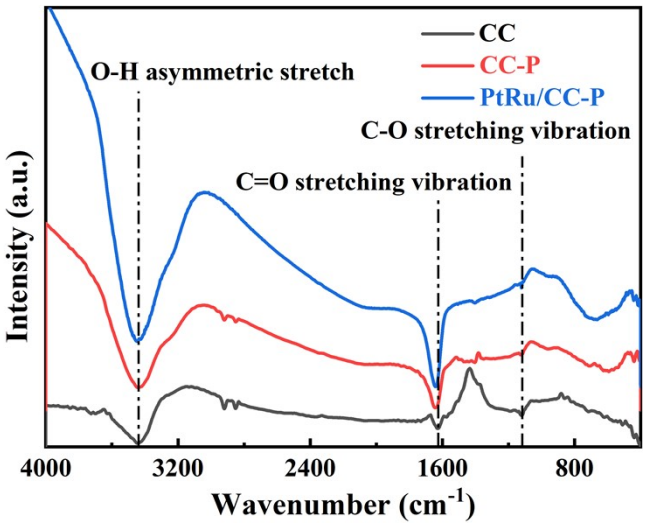

Fig. S5. FT-IR spectra of PtRu/CC-P, CC-P and CC.

The peaks located at 3445, 1623 and 1140 cm^{-1} belong to O-H asymmetric stretch, C=O stretching vibration and C-O stretching vibration [11, 15], respectively, in Fourier transform infrared spectra (FT-IR) of bare CC, CC-P and PtRu/CC-P.

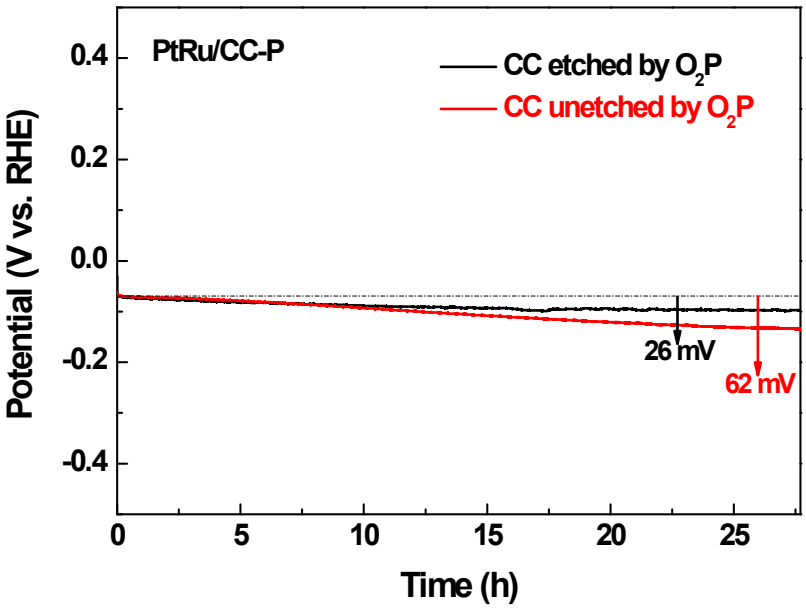

Fig. S6. the chronopotentiometric curves of PtRu/CC-P etched and unetched by O_2 plasma at 10 mA·cm^{-2} in 1M KOH

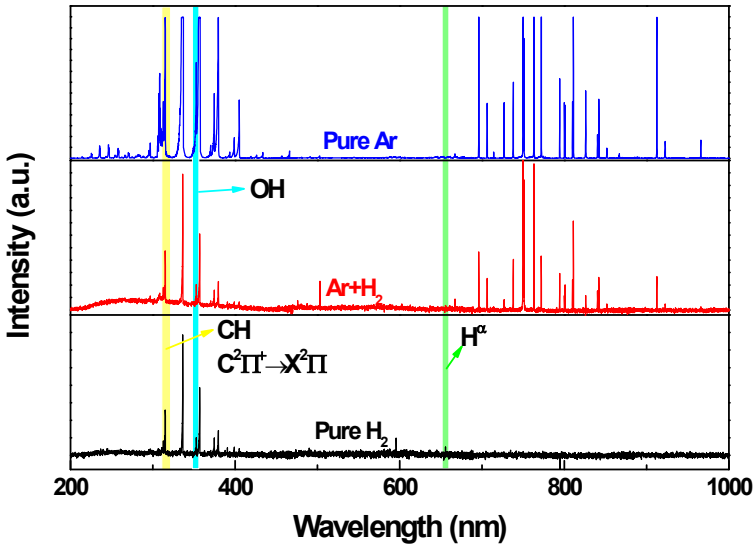

Fig. S7. The optical emission spectra of DBD cold plasma under discharge gases of pure Ar, 50%H_2/Ar and pure H_2.

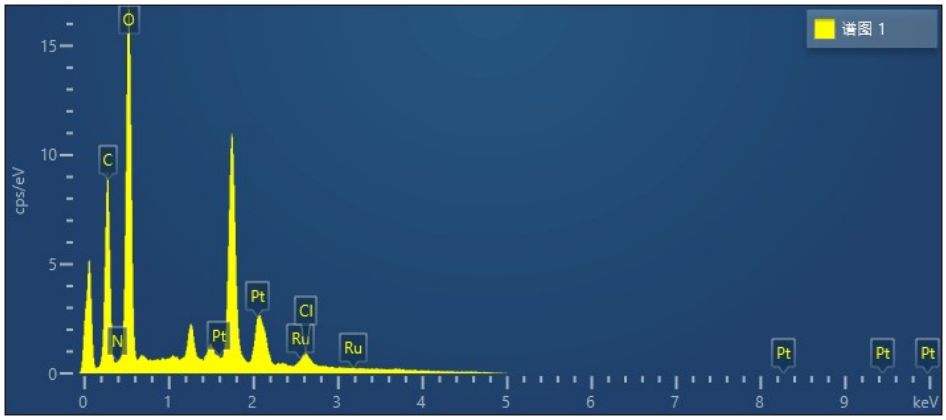

Fig. S8. EDX analysis of PtRu/CC-P.

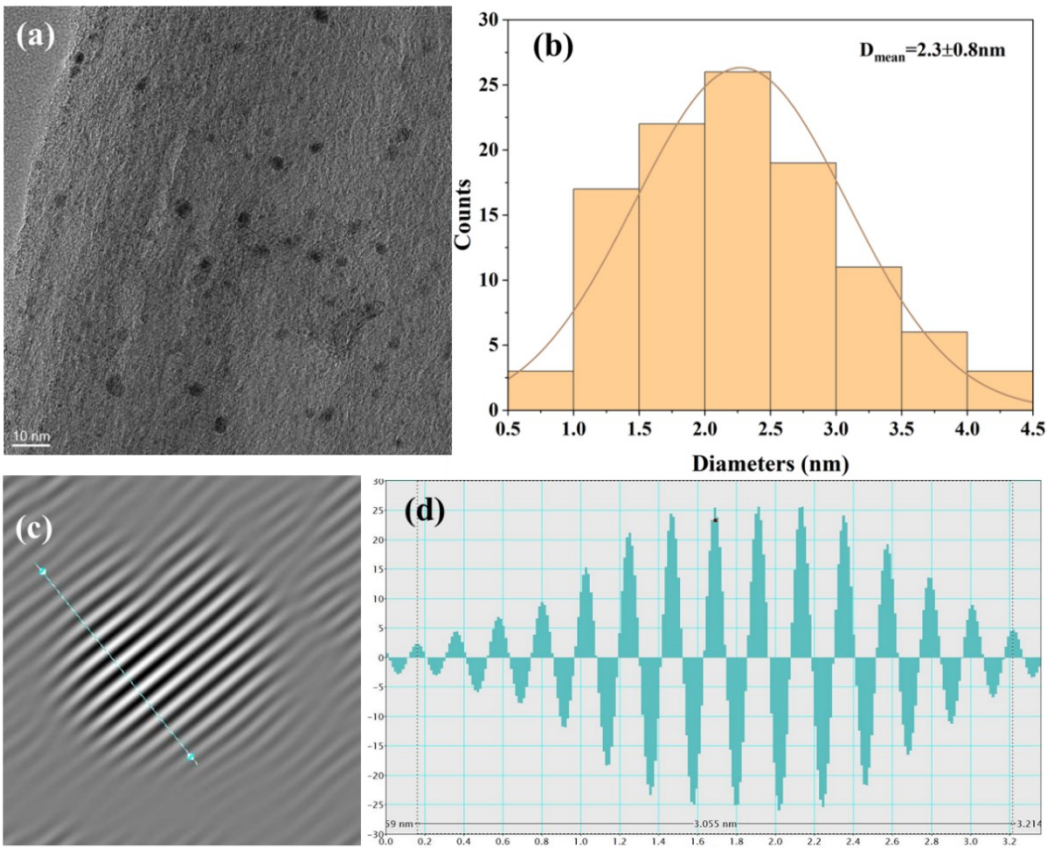

Fig. S9. (a) TEM image, (b) size distribution histogram of the nanoparticles, (c) IFFT image, and (d) atomic intensity profile of PtRu/CC-P.

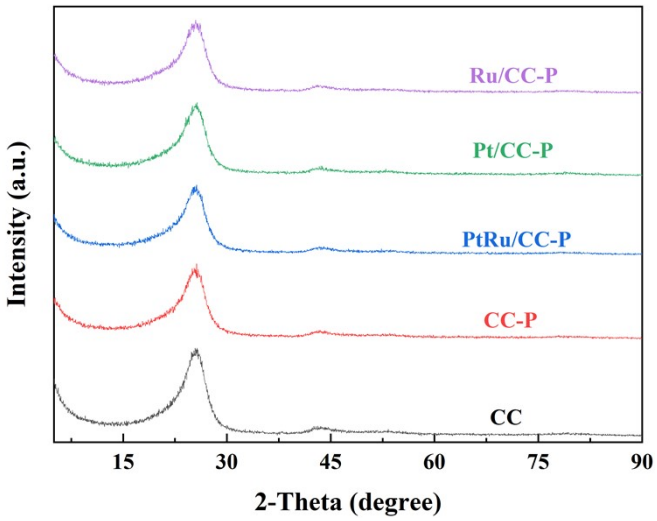

Fig. S10. XRD patterns of CC, CC-P, PtRu/CC-P, Pt/CC-P and Ru/CC-P.

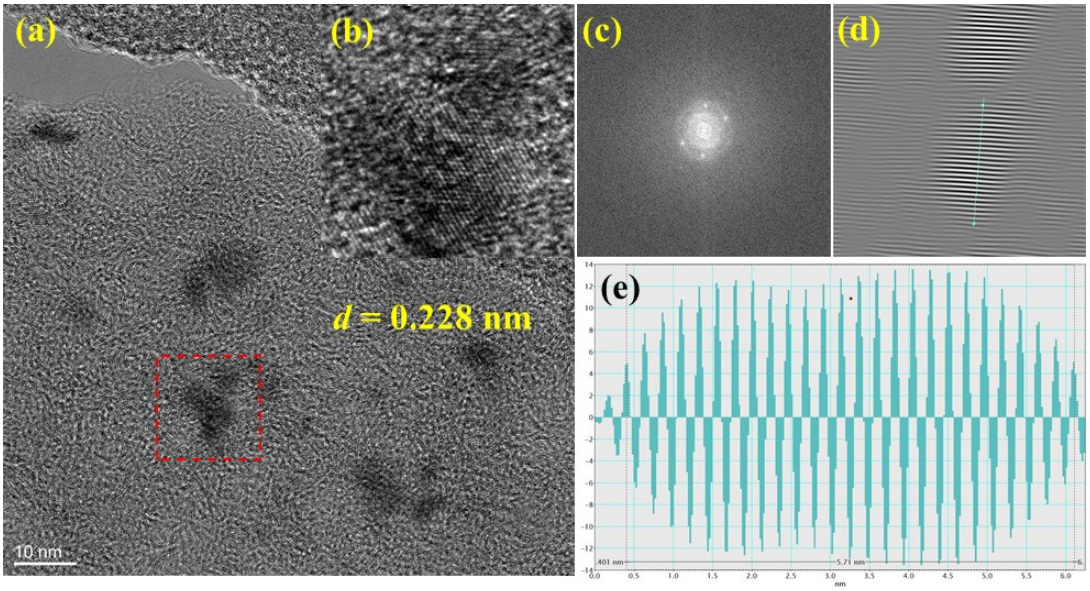

Fig. S11. (a) TEM image, (b) HRTEM image, (c) FFT and (d) IFFT, and (e) atomic intensity profile of Pt/CC-P.

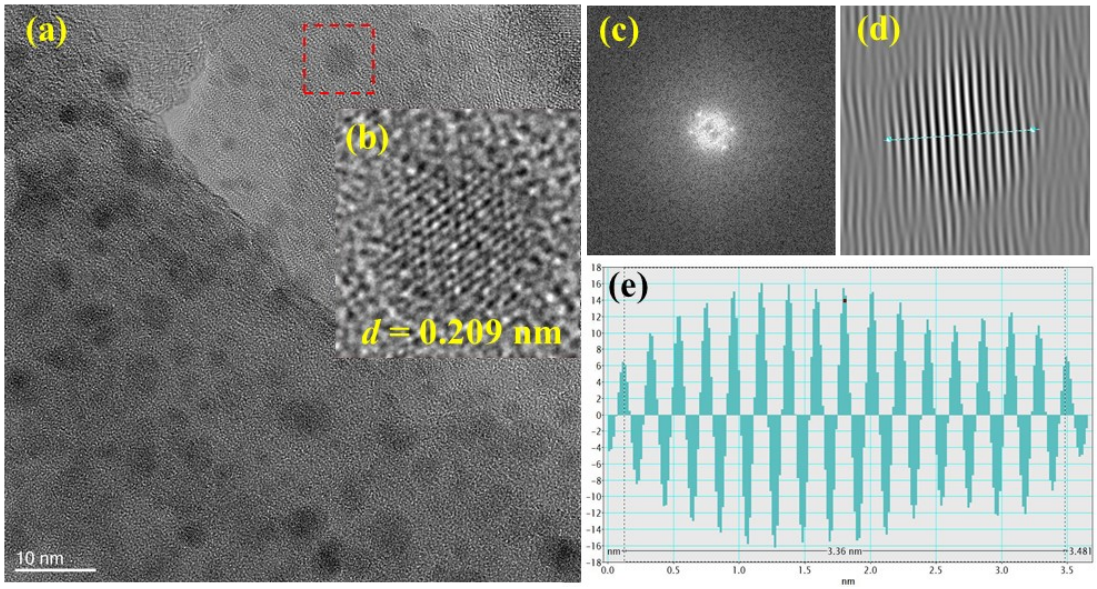

Fig. S12. (a) TEM image, (b) HRTEM image, (c)FFT and (d) IFFT, and (e) atomic intensity profile of Ru/CC-P.

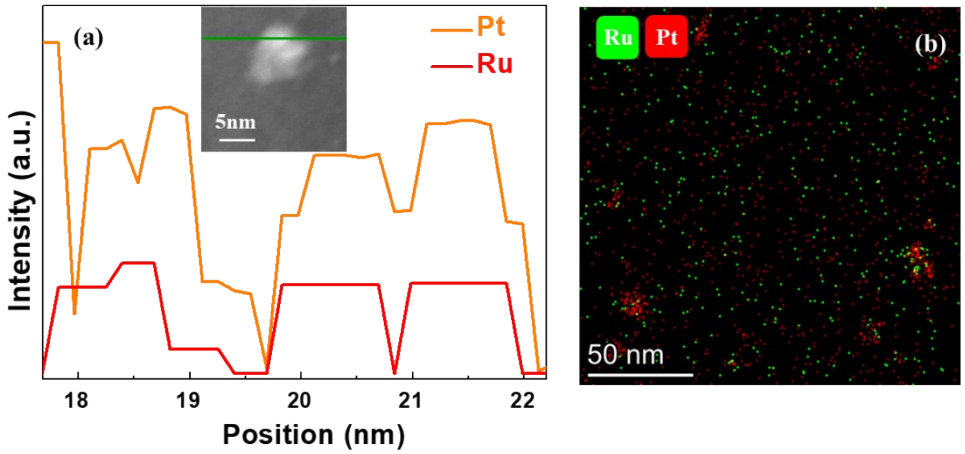

Fig. S13. (a) Line scan profile, and (b) EDS elemental mapping image of PtRu/CC-P.

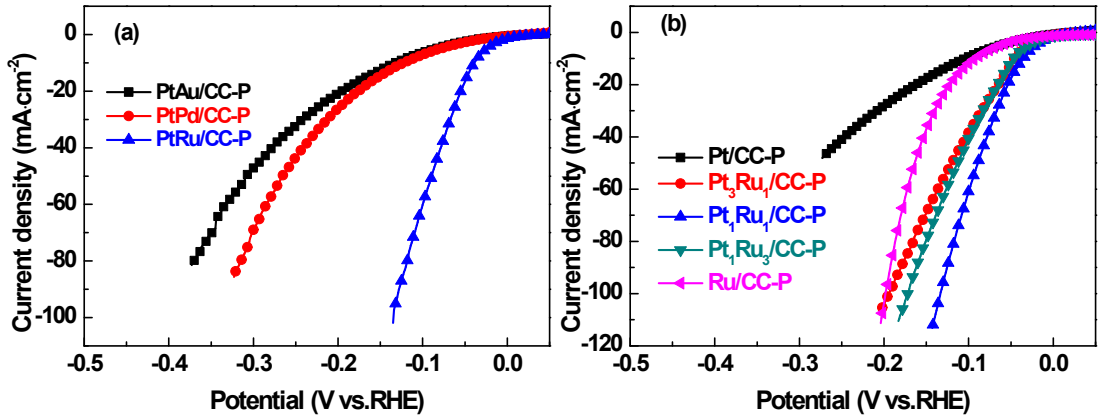

Fig. S14. (a) Electrocatalytic HER polarization curves of the Pt-based bimetallic catalysts prepared by cold plasma in 1M KOH solution. (b) Electrocatalytic HER polarization curves of the PtRu/CC-P catalysts with various Pt/Ru ratios prepared by cold plasma in 1M KOH solution.

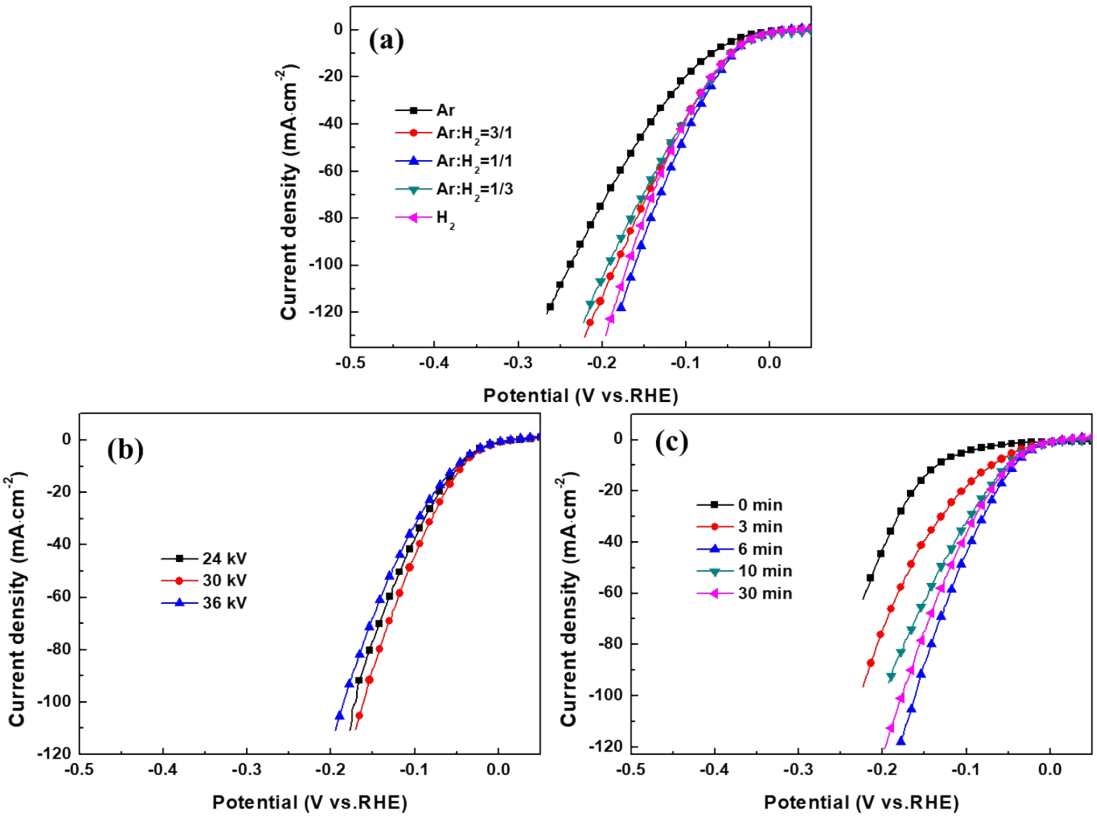

Fig. S15. Electrocatalytic HER polarization curves of PtRu/CC-P prepared by cold plasma under different plasma parameters in 1M KOH solution: (a) the effect of H_2/Ar ratio on the HER performance of PtRu/CC-P, (b) the effect of discharge voltage on the HER performance of PtRu/CC-P, (c) the effect of discharge time on the HER performance of PtRu/CC-P.

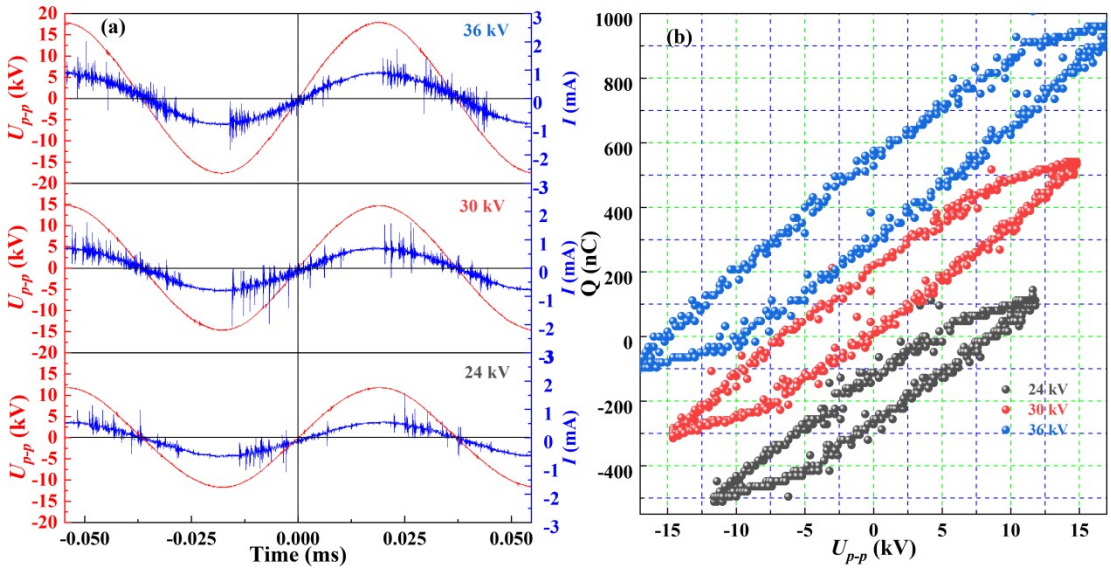

Fig. S16. (a) Discharge voltage and current waveforms, and (b) the corresponding Lissajous Figures of 50%H_2/Ar cold plasma at different discharge voltages (24, 30 and 36 kV) with a discharge frequency of 13.6 kHz for treating PtRu/CC-P.

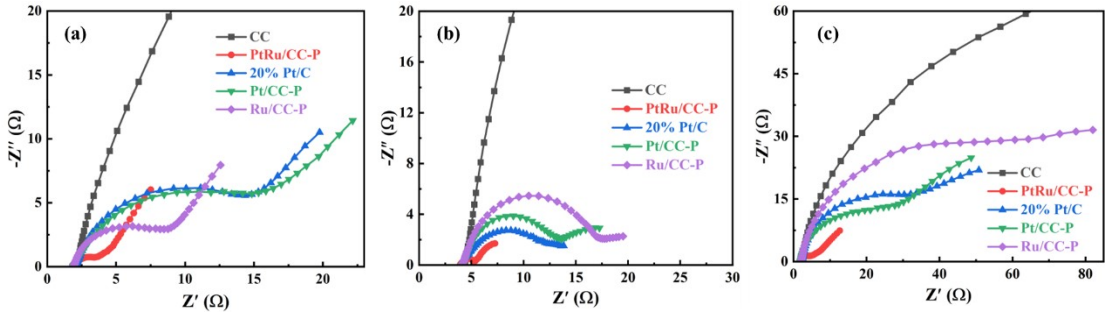

Fig. S17. The EIS plots of CC, PtRu/CC-P, 20%Pt/C, Pt/CC-P and Ru/CC-P in (a) alkaline, (b) neutral, and (c) acidic media.

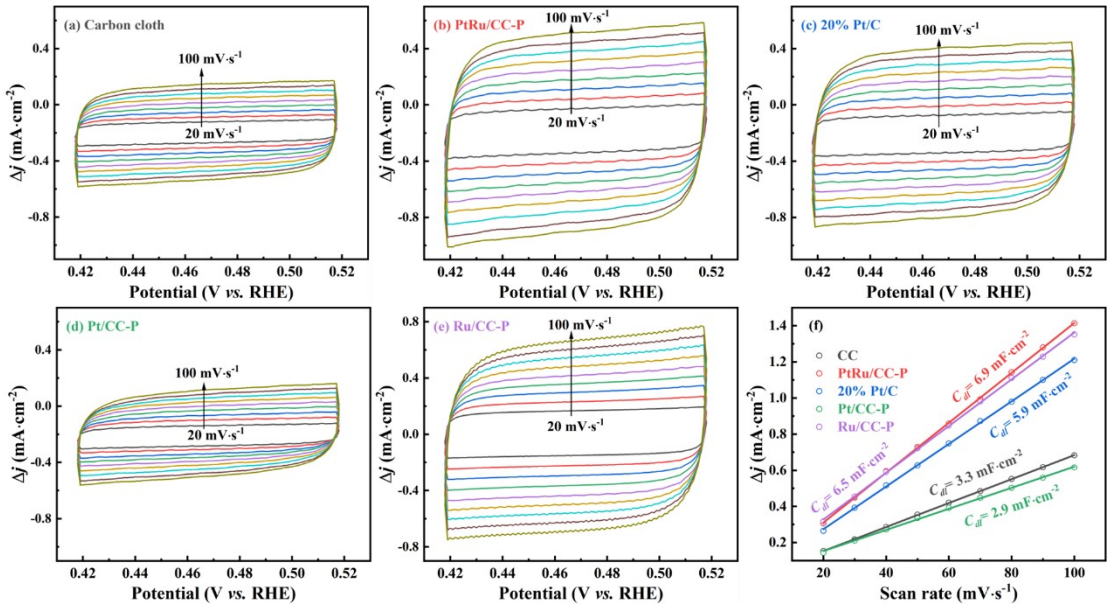

Fig. S18. CV curves of (a) CC, (b) PtRu/CC-P, (c) 20%Pt/C, (d) Pt/CC-P, (e) Ru/CC-P in 1.0 M KOH, and corresponding double-layer capacitance (C_{dl}) values (f).

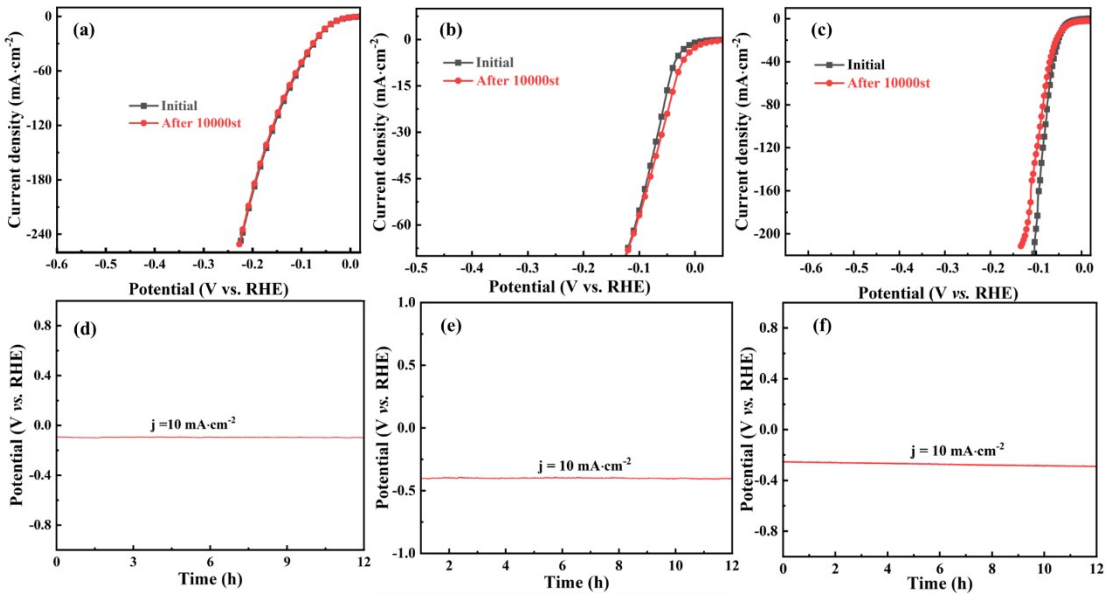

Fig. S19 (a-c) Polarization curves for PtRu/CC-P before and after 5000 CV cycles, and the chronopotentiometric curves of PtRu/CC-P at 10 mA·cm^{-2} in (d) alkaline, (e) neutral, and (f) acidic media.

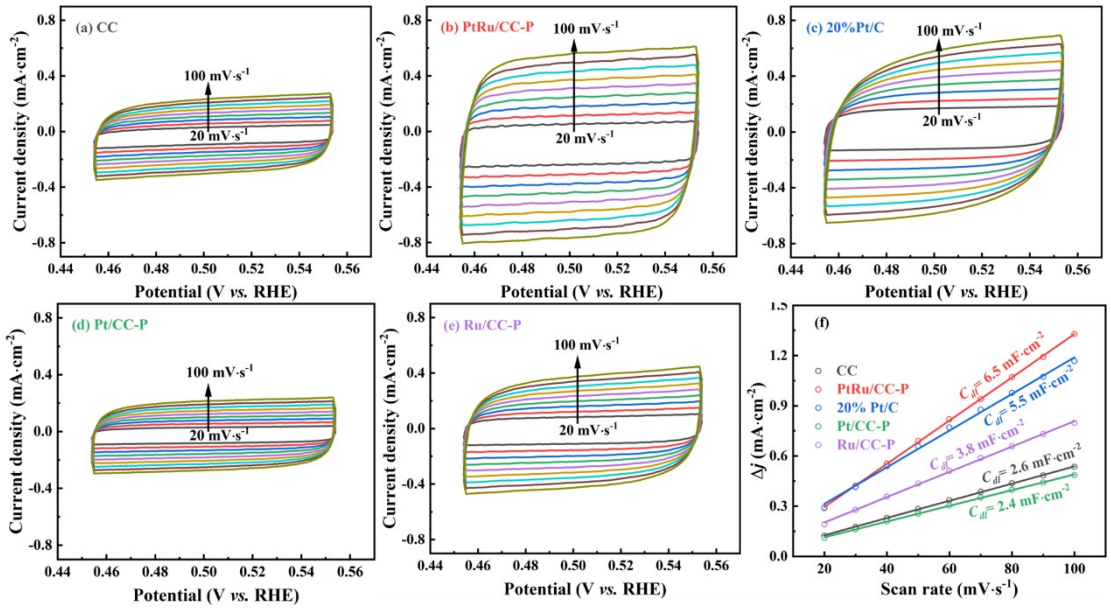

Fig. S20. CV curves of (a) CC, (b) PtRu/CC-P, (c) 20%Pt/C, (d) Pt/CC-P, (e) Ru/CC-P in 1.0 M PBS, and corresponding C_{dl} values (f).

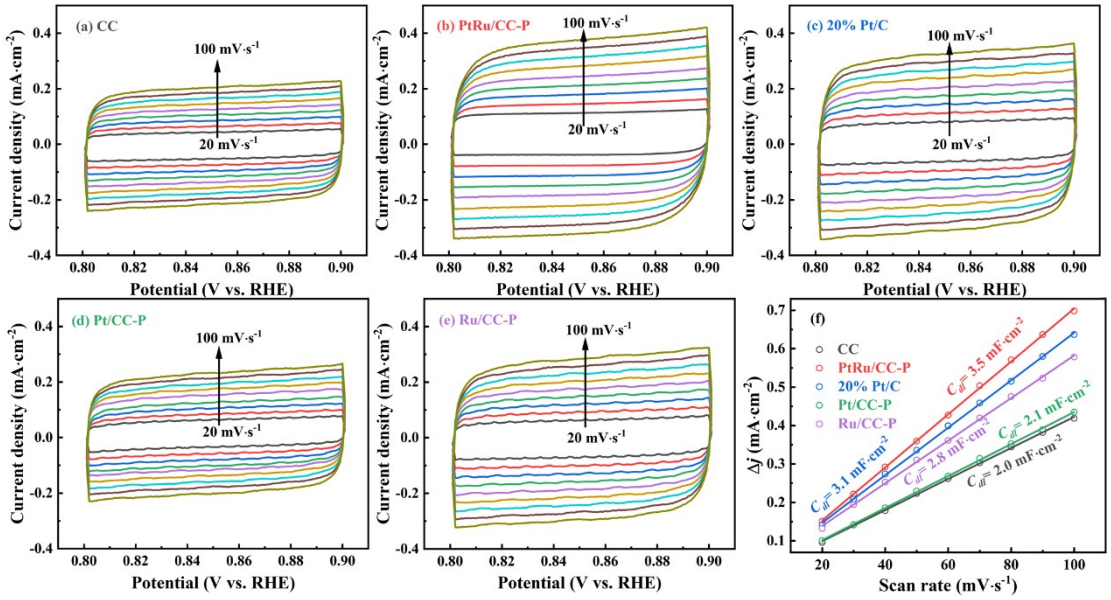

Fig. S21. CV curves of (a) CC, (b) PtRu/CC-P, (c) 20%Pt/C, (d) Pt/CC-P, (e) Ru/CC-P in 0.5 M H_2SO_4, and corresponding C_{dl} values (f).

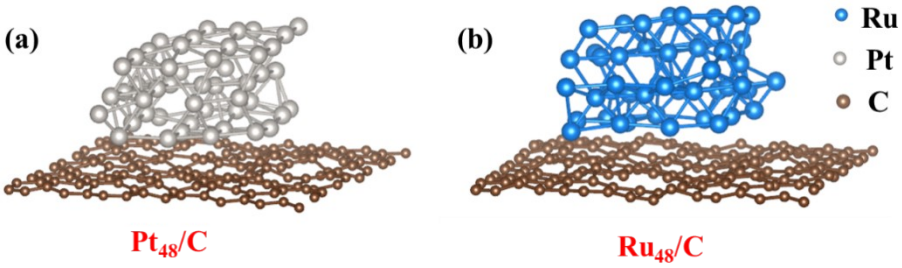

Fig. S22. Constructed structure model of (a) Pt_{48}/C and (b) Ru_{48}/C

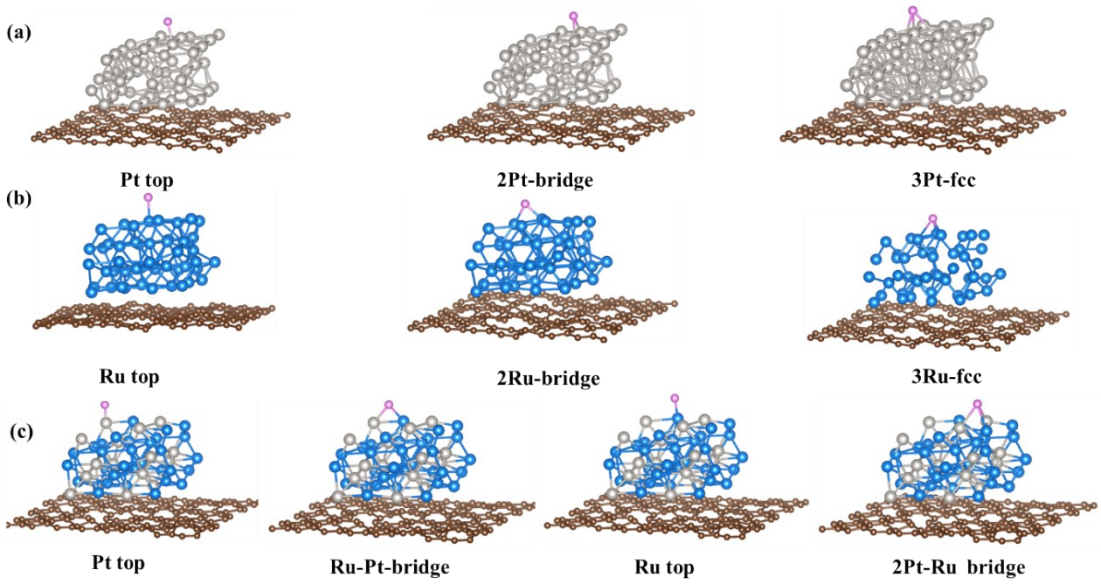

Fig. S23. Optimized structures of H adsorbed on (a) Pt top, 2 Pt-bridge, 3 Pt-fcc sites for Pt_{48}, (b) Ru top, 2Ru-bridge, 3Ru-fcc sites for Ru_{48}, (c) Pt top, Ru-Pt-bridge, Ru top sites for $Pt_{16}Ru_{32}$.

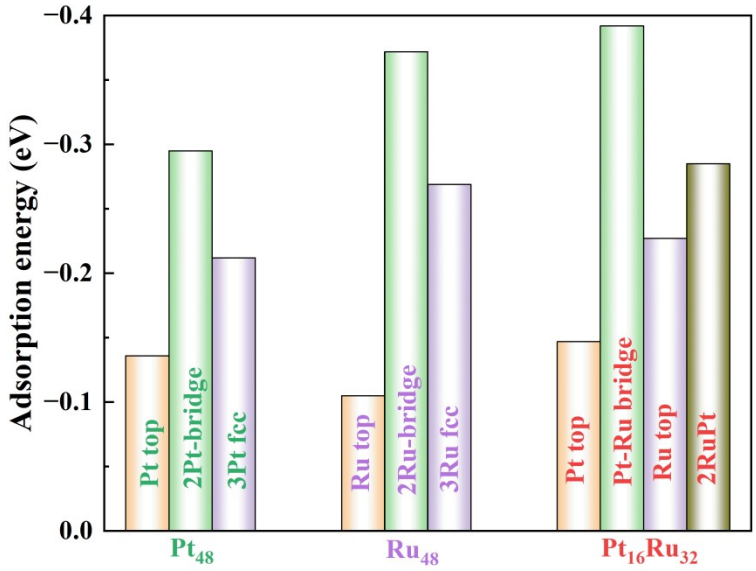

Fig. S24. Calculated H adsorption energies on different adsorption sites of Pt_{48}, Ru_{48} and $Pt_{16}Ru_{32}$

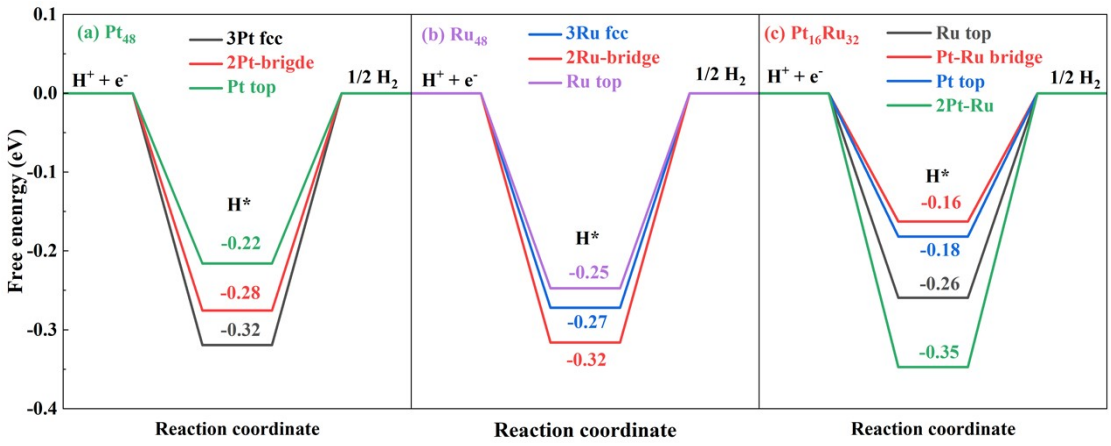

Fig. S25. Calculated free-energy diagram of HER on different adsorption sites of (a) Pt_{48}, (b) Ru_{48} and (c) $Pt_{16}Ru_{32}$.

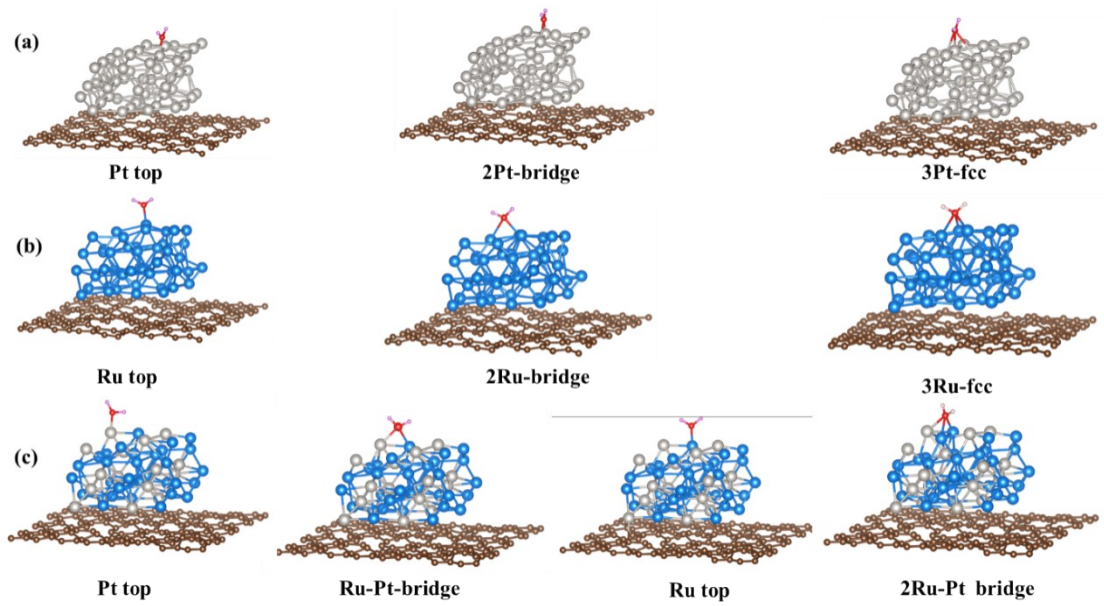

Fig. S26. Water adsorption configurations of (a) Pt top, 2 Pt-bridge, 3 Pt-fcc sites for Pt_{48}, (b) Ru top, 2Ru-bridge, 3Ru-fcc sites for Ru_{48} (c) Pt top, Ru-Pt-bridge, Ru top sites for $Pt_{16}Ru_{32}$.

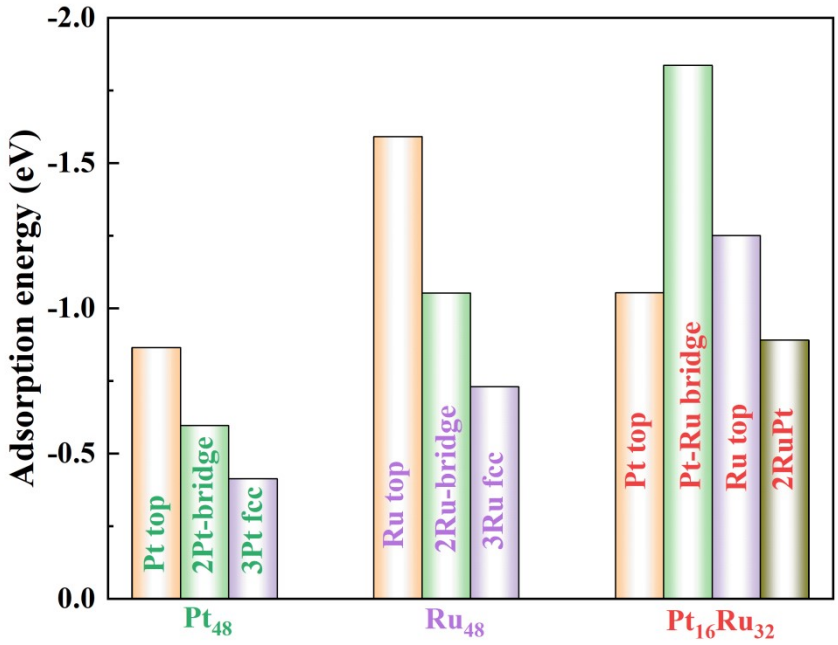

Fig. S27. Calculated H_2O adsorption energies on different adsorption sites of Pt_{48}, Ru_{48} and $Pt_{16}Ru_{32}$.

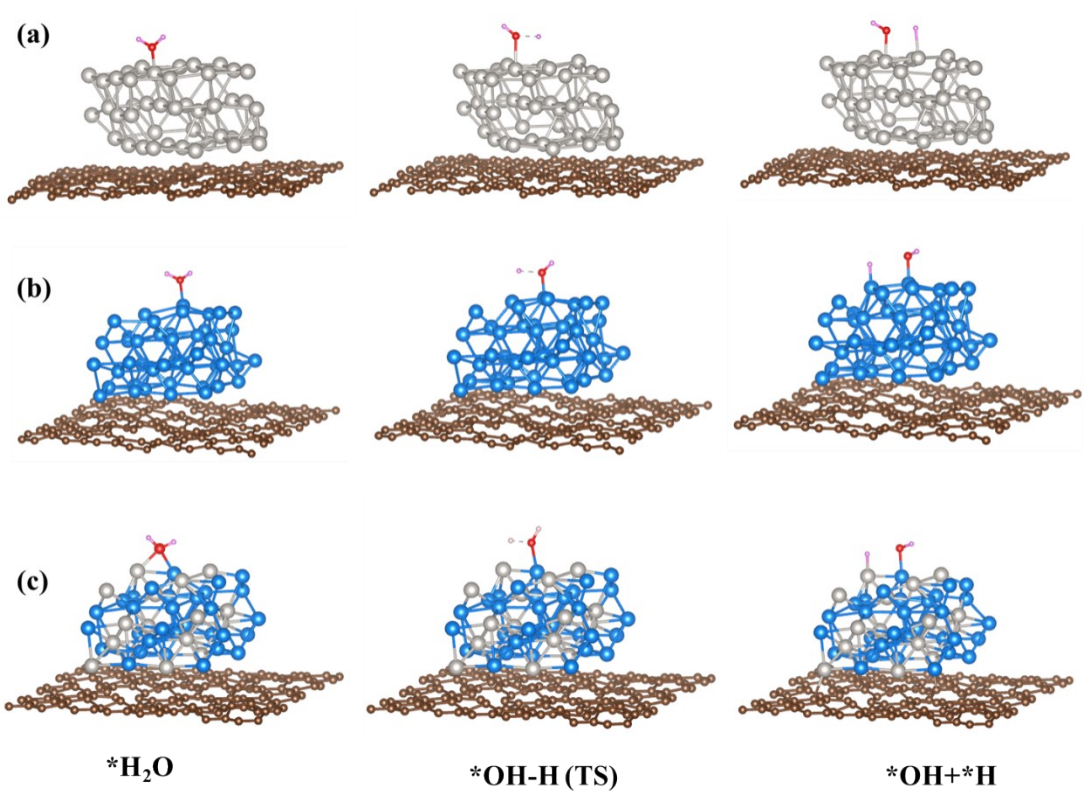

Fig. S28. Water adsorption and dissociation configurations of (a) Pt top sites for Pt_{48}, (b) Ru top sites for Ru_{48}, (c) Ru-Pt-bridge sites for $Pt_{16}Ru_{32}$.

Table S1. Metal contents obtained from ICP for PtRu/CC-P, Pt/CC-P and Ru/CC-P catalysts, as well as atomic ratios of Pt/Ru of PtRu/CC-P.

Catalyst	Pt loading (wt %)	Ru loading (wt %)	Atomic ratios of Pt/Ru [a)]	Atomic ratios of Pt/Ru [b)]
PtRu/CC-P	0.047	0.049	1/2	1/2
Pt/CC-P	0.092	—	—	—
Ru/CC-P	—	0.091	—	—

[a)] obtained from ICP; [b)] obtained from XPS.

Table S2. The HER performance comparison of the representative catalysts in alkaline electrolyte.

Catalyst	Mass loading	$\eta_{j=10}$ (mV)	Tafel slope (mV·dec^{-1})	TOF (H_2·s^{-1})	Mass activity (A·mg^{-1})	Reference
PtRu/CC-P	0.05 wt%	44	45.1	2.6@100 mV	3.77@100 mV	This work
Pt/C	20 wt%	55	56.4	1.06@100 mV	1.05@100 mV	This work
$Pt_{0.47}$-Ru/Acet	0.47 wt%	17	66.6	0.7@100 mV	1.33@100 mV	*Chem. Eng. J.*, 2022, **448**, 137611
Pt_3Co@NCNT	25.2 wt%	36	34.8	0.94 @100 mV		*Angew. Chem. Int. Ed.*, 2021, **60**, 19068
$CoPt_3$@Co_2P/ Co@NCNT	13.1 wt%	19	48	1.11 @100 mV		*Small*, 2021, **17**, 2104656
Pt/MOF-O	20.4μg·cm^{-2}	66	101.6		1.33@140 mV	*J. Am. Chem. Soc.*, 2021, **143**, 16512
Pt_1-Mo_2C-C	0.7 wt%	155	64		7.14@155 mV	*J. Energy Chem.*, 2021, **57**, 371
PtRu/mCNTs	0.57 wt%	15	33.5		3.35@100 mV	*Energy Environ. Sci.*, 2022, **15**, 102
Dr-Pt	19.5 μg·cm^{-2}	26	52		1.16@50 mV	*Adv. Mater.*, 2021, **34**, 2106973
Pt_{SA}–Ni_3S_2@Ag NWs	1.47 wt%	33	34.70	2.91@95 mV	7.6@150 mV	*Adv. Sci.*, 2021, **8**, 2100347
PtRu@C_2N	19 wt %	59	63	4.23@300 mV		*Chem. Eng. J.*, 2022, **428**, 131085.
PtRu/EC-700	3.2 wt %	18 mV	44.54	0.229 @30 mV	0.863@50 mV	*Nanoscale*, 2021, **13**, 10044
Pt/np-$Co_{0.85}Se$	1.03 wt %	58	39		1.28@100 mV	*Nat. Commun.*, 2019, **10**, 1743
Pt-CoS_2/CC	7.3 wt%	24	82		2.1@100 mV	*Adv. Energy Mater.*, 2018, **8**, 1800935
Pt-NiFe LDH-ht/CC	1.65 wt%	101	127		0.244@101 mV	*Nano Energy,* 2017, **39**, 30
α-MoC_{1-x}/Pt	2.7 wt%	67	55			*Adv. Sci.*, 2019, **6**, 1802135

Pt@PCM	0.53 wt%	139	73.6			*Sci. Adv.*, 2018, **4**, eaao6657
Pt_{SA}–$Co(OH)_2$@Ag NW	2.8 wt%	29	35.72		1.6	*Energy Environ. Sci.*, 2020, **13**, 3082
Mo_2C@NC@Pt	7.49 wt%	47	57			*ACS Appl. Mater. Inter.*, 2019, **11**, 4047
Pt/Ni-SP	3.5 wt%	76	28.3		1.11@50 mV	*Sci Rep-UK*, 2018, **8**, 2986
Pt−$Co(OH)_2$/CC	5.7 wt%	32	70			*ACS Catal.*, 2017, **7**, 7131
PtNiP NWs	30.6 $\mu g \cdot cm^{-2}$	9	30		6.27@70 mV	*Appl. Catal. B-Environ.*, 2022, **301**, 120754
Pt@DG	1.57 wt%	37	119	6.74@100 mV	6.78@100 mV	*J. Am. Chem. Soc.*, 2022, **144**, 2171
PtFe-mix	58 at%	28	42	12.5@100 mV		*Small*, 2022, **18**, 2106947
NF-Na-Fe-Pt	0.6 wt%	31	35.98		6.9@100 mV	*Appl. Catal. B-Environ.*, 2021, **297**, 120395
Pt_{SA}-NiO/Ni	1.14 wt%	26	27.07	5.71 @50 mV	20.6@100 mV	*Nat. Commun.*, 2021, **12**, 3783
BPIr_be	7.33 wt%	1.98	91	26@100 mV		*Adv. Mater.*, 2021, **33**, 2104638
Pt/Ni ASs/C	2 $\mu g \cdot cm^{-2}$	28	47.0	11.4@50 mV	30.2@100 mV	*Nano Lett.*, 2021, **21**, 9381
Pt_1/N-C	2.5 wt%	46	36.8	1.89 @50 mV		*Nat. Commun.*, 2020, **11**, 1029

Table S3. The HER performance comparison of the representative catalysts in neutral electrolyte.

Catalyst	Mass loading	$\eta_{j=10}$ (mV)	Tafel slope (mV·dec^{-1})	TOF (H_2·s^{-1})	Mass activity (A·mg^{-1})	Reference
PtRu/CC-P	0.05 wt%	42	39.5	2.72@100 mV	3.96@100 mV	This work
Pt/C	20 wt%	60	40.8	1.31@100 mV	1.29@100 mV	This work
$Pt_{0.47}$-Ru/Acet	0.47 wt%	8	94.4		0.85@100 mV	*Chem. Eng. J.*, 2022, **448**, 137611
BPIr_be	7.33 wt%	~320	160	~0.6@300 mV		*Adv. Mater.*, 2021, **33**, 2104638
Pt/np-$Co_{0.85}Se$	1.03 wt %	55	35	3.93@100 mV	1.32@100 mV	*Nat. Commun.*, 2019, **10**, 1743
Pt_{SA}-NiO/Ni	1.14 wt %	27	31.94			*Nat. Commun.*, 2021, **12**, 3783
PtRu/mCNTs	0.57 wt%	17	48.7			*Energy Environ. Sci.*, 2022, **15**, 102
Pt-$Co(OH)_2$/CC	5.7wt%	84				*ACS Catal.*, 2017, **7**, 7131
Mo_2C@NC@Pt	7.49 wt%	8	33			*ACS Appl. Mater. Inter.*, 2019, **11**, 4047
PtSi		66	47			*Adv. Energy Mater.*, 2022, 2200293

Table S4. The HER performance comparison of the representative catalysts in acidic electrolyte.

Catalyst	Mass loading	η_{10} (mV)	Tafel slope (mV·dec^{-1})	TOF (H_2·s^{-1})	Mass activity (A·mg^{-1})	Reference
PtRu/CC-P	0.05 wt%	42	32.5	9.63@100 mV	13.96@100 mV	This work
Pt/C	20 wt%	55	33.3	7.27@100 mV	7.19@100 mV	This work
PtRu@C_2N	19 wt%	52	31	2.72@300 mV		*Chem. Eng. J.*, 2022, **428**, 131085
$Pt_{0.47}$-Ru/Acet	0.47 wt%	28	33.4		2.63@100 mV	*Chem. Eng. J.*, 2022, **448**, 137611
Pt_x/TiO_2 NTs@3D-Ti	2.5 μg·cm^{-2}	53	37		4.55@100 mV	*Mater. Today Energy*, 2022, 101042
PtCu/WO_3 @CF	4.3 μg·cm^{-2}	41	45.9	10.9@100 mV	10.86@100 mV	*Adv. Funct. Mater.*, 2022, 2112207
Pt/MXene	2.9 wt%	34	29.7	10.66@200 mV	1.847@50 mV	*Adv. Funct. Mater.*, 2022, 2110910
Pt_3Co@NC NT	25.2 wt%	42	27.2	1.95@100 mV		*Angew. Chem. Int. Ed.*, 2021, **60**, 19068
Pt/MOF-O	20.4 μg·cm^{-2}	28	24.4		0.97@40 mV	*J. Am. Chem. Soc.*, 2021, **143**, 16512
Pt/VS_2/CP	0.65 wt %	77	40.13		9.81@200 mV	*ACS Nano*, 2020, **14**, 5600
Pt/def-WO_3@CFC	15.9 μg·cm^{-2}	42	73	1.11@70 mV		*J. Mater. Chem. A*, 2019, **7**, 6285
Pt@Co SAs-ZIF-NC	5.01 wt%	27	21		1.5@30 mV	*Nano Energy*, 2021, **88**, 106221
CPt@ZIF-67	5 wt%	50	27.1	2.94@100 mV	0.87 @10 mV	*J. Mater. Chem. A*, 2019, **7**, 6543
Pt/np-$Co_{0.85}Se$	1.03 wt %	58	26		13.57@100 mV	*Nat. Commun.*, 2019, **10**, 1743
Pt@PCM	0.53 wt%	105	63.7	43.6@500 mV		*Sci. Adv.*, 2018, **4**, eaao6657
Pt/GNs	14.7 wt.%	25	33	0.854@30 mV	2.24@30 mV	*Carbon*, 2018, **137**, 405
Pt_1/N-C	2.5 wt%	19	14.2	22.07@50mV		*Nat. Commun.*, 2020, **11**, 102
$Mo_2TiC_2T_x$ –Pt_{SA}	1.2 wt%	30	30		8.3@77mV	*Nat. Catal.*, 2018, **1**, 985
Pt/SnS_2	0.373 wt	117	69			*ACS Appl. Mater.*

	%					*Inter.*, 2017, **9**, 37750
Pt-Mo_2C/TiO_2 NTAs	13 $\mu g \cdot cm^{-2}$	67	39.3			*Appl. Surf. Sci.*, 2020, **509**, 144679
Pt/3DSG	3.1 wt%	112	53.7			*Int. J. Hydrogen Energ.*, 2018, **43**, 23231
PtNW/SWNT-O_3	3.9 wt%	18	107			*Appl. Catal. B-Environ.*, 2020, **265**, 118582
Pt@NHPCP	3.6 wt%	57	27			*Nano Energy*, 2017, **40**, 88
PtRu/mCNTs	0.57 wt %	28	22.6			*Energy Environ. Sci.*, 2022, **15**, 102
α-MoC_{1-x}/Pt	2.7 wt%	30	31			*Adv. Sci.*, 2019, **6**, 1802135
Pt@DG	1.57 wt%	30	48	26.41@ 100 mV	26.05@100 mV	*J. Am. Chem. Soc.*, 2022, **144**, 2171
Pt_2Sr/NC	9.32 wt%	27	26		0.64@30 mV	*J. Energy Chem.*, 2022, **64**, 315
Pt/MoS_2NTA/Ti_3C_2	0.13 wt%	32	35	47.0@100 mV	46.5@100 mV	*Small*, 2022, 2105129
Pt_1/Co_1NC	0.4 wt%	4.15	17	32.86@ 20 mV	32.4@20 mV	*Appl. Catal. B-Environ.*, 2022, **301**, 120830
Pt-Ru/CNT	4.94 at%	12	23	25.1@100 mV		*Small*, 2021, **18**, 2104559
BPIr_be	7.33 wt%	25	30.9	22@100 mV		*Adv. Mater.*, 2021, **33**, 2104638
Pt-CoO/p-CNF	1.6 wt%	26	31.5		4.42@30 mV	*J. Energy Chem.*, 2021, **52**, 33
Pt/WGA	0.8 wt%	42	30	29.05@ 50 mV		*Small*, 2021, **17**, 2102159
PtN_x/TiO_2	1.4 wt %	67	34		136.4@100 mV	*Nano Energy*, 2020, **73**, 104739
Pt SAs/DG	2.1 wt %	23	25		26.2@50 mV	*J. Am. Chem. Soc.*, 2019, **141**, 4505
Pt SASs/AG	0.44 wt%	12	29.33		22.4@50 mV	*Energy Environ. Sci.*, 2019, **12**, 1000
Pt_1/OLC	0.27wt %	38	36	40.78@ 100 mV	7.40@38 mV	*Nat. Energy*, 2019, **4**, 512

Reference

1. C. Hu, E. Song, M. Wang, W. Chen, F. Huang, Z. Feng, J. Liu and J. Wang, *Adv. Sci.*, 2021, **8**, 2001881.
2. Y. Shi, D. Zhang, H. Huang, H. Miao, X. Wu, H. Zhao, T. Zhan, X. Chen, J. Lai and L. Wang, *Small*, 2022, **18**, 2106947.
3. Q. Chen, B. Wei, Y. Wei, P. Zhai, W. Liu, X. Gu, Z. Yang, J. Zuo, R. Zhang and Y. Gong, *Appl. Catal. B-Environ.*, 2022, **301**, 120754.
4. S. Jiao, M. Kong, Z. Hu, S. Zhou, X. Xu and L. Liu, *Small*, 2022, DOI: 10.1002/smll.202105129, e2105129.
5. R. Ding, Q. Chen, Q. Luo, L. Zhou, Y. Wang, Y. Zhang and G. Fan, *Green Chem.*, 2020, **22**, 835-842.
6. Y. Feng, W. Feng, J. Wan, J. Chen, H. Wang, S. Li, T. Luo, Y. Hu, C. Yuan, L. Cao, L. Feng, J. Li, R. Wen and J. Huang, *Appl. Catal. B-Environ.*, 2022, **307**, 121193.
7. L. Dai, Y. Shen, J. Z. Chen, L. Zhou, X. Wu, Z. Li, J. Wang, W. Huang, J. T. Miller, Q. Wang, A. Cao and Y. Wu, *Small*, 2022, **18**, 2105226.
8. L. Zhang, H. Jang, Y. Wang, Z. Li, W. Zhang, M. G. Kim, D. Yang, S. Liu, X. Liu and J. Cho, *Adv Sci (Weinh)*, 2021, **8**, e2004516.
9. N. Wang, S. Ning, X. Yu, D. Chen, Z. Li, J. Xu, H. Meng, D. Zhao, L. Li, Q. Liu, B. Lu and S. Chen, *Appl. Catal. B-Environ.*, 2022, **302**, 120838.
10. L. Liu, Y. Wang, Y. Zhao, Y. Wang, Z. Zhang, T. Wu, W. Qin, S. Liu, B. Jia, H. Wu, D. Zhang, X. Qu, M. Chhowalla and M. Qin, *Adv. Funct. Mater.*, 2022, DOI: 10.1002/adfm.202112207, 2112207.
11. X. Wu, W. Xu, Z. Wang, H. Li, M. Wang, D. Zhang, J. Lai and L. Wang, *Chem. Eng. J.*, 2022, **431**, 133247.
12. K. Wang, M. Xu, Y. Gu, Z. Gu, J. Liu and Q. H. Fan, *Nano Energy*, 2017, **31**, 486-494.
13. D. X. Yang, W. Q. Hou, Y. J. Lu, X. Q. Wang, W. L. Zhang and Y. F. Chen, *ACS Sustain. Chem. Eng.*, 2019, **7**, 13031-13040.
14. B. Yu, F. Qi, Y. Chen, X. Wang, B. Zheng, W. Zhang, Y. Li and L.-C. Zhang, *ACS Appl. Mater. Inter.*, 2017, **9**, 30703-30710.
15. X. Yan, H. Li, J. Sun, P. Liu, H. Zhang, B. Xu and J. Guo, *Carbon*, 2018, **137**, 405-410.